# PHYSICOCHEMICAL PROPERTIES AND APPLICATION OF NICKEL NANOPARTICLES IMMOBILIZED ON PRISTINE FILTER PAPER AND MODIFIED FILTER PAPER: A COMPARATIVE STUDY

Tan Shi Nin, Yuen Mei Lian*, Ros Azlinawati Ramli and Muhammad Farid Rafiq Abdul Manaf

Faculty of Industrial Sciences and Technology, Universiti Malaysia Pahang Al-Sultan Abdullah, Lebuh Persiaran Tun Khalil Yaakob, 26300 Kuantan, Pahang, Malaysia.

*yuenm@umpsa.edu.my

**Abstract**. Chitosan and cellulose are ubiquitous and biodegradable polysaccharides. With the presence of amino (-$NH_2$) and hydroxyl (-OH) groups, chitosan and cellulose are introduced as supporting materials for metal nanoparticles. This study aimed to investigate and compare the physicochemical properties of nickel nanoparticles (NiNPs) immobilized on two different substrates, which are pristine filter paper (FP) and chitosan-filter paper (CS-FP). Their photodegradation efficiency of methylene blue (MB) under UV irradiation were determined by parameters such as the initial concentration of MB, the photocatalyst dosage, and the concentration of the reducing agent. The presence of chitosan impact on the composition of NiNPs was revealed through the application of SEM-EDX and FTIR analysis. Additionally, increasing the photocatalyst dosage from 0.2 g to 0.6 g resulted in the photocatalytic degradation of MB by NiNPs/FP and NiNPs/CS-FP increasing from 42.8 % to 68.7 % and 22.4 % to 47.6 %, respectively. In addition, it was demonstrated that the photodegradation efficiency of NiNPs/FP and NiNPs/CS-FP was decreased from 67.4 % to 62.8 % and 61.4 % to 38.7 %, respectively, by raising the initial concentration of MB (10-50 ppm). As the reducing agent concentration (0-0.5 M) increases, the photodegradation efficiency of NiNPs/FP and NiNPs/CS-FP increase from 24.4 % to 98.2 % and 4.6 % to 64.4 %, respectively. It can be concluded that both NiNPs/FP and NiNPs/CS-FP have good points in different aspects. Taken together, the results of this study may contribute to an ideal nanoparticle immobilization matrix. Consequently, its application in the photodegradation of dyes may achieve the third goal of Sustainable Development Goal (SDG) 6, which is to increase global water recycling and safe reuse by minimizing the amount of untreated wastewater globally.

**Keywords:** Chitosan, cellulose, nickel nanoparticles, photodegradation, methylene blue

**Article Info**

Received 16th December 2023
Accepted 13th May 2024
Published 12th June 2024

ISSN: 1823-7010, eISSN: 2600-7444

## 1. INTRODUCTION

Industrialization and urbanization have generated a massive amount of waste and pollutants, especially in economically developing nations. The textile sector is one of the major industries that contribute to a significant pollution level, accounting for about a fifth of textile effluent from the total industrial wastewater produced in Malaysia [1]. Textile effluent composition includes a high concentration of total dissolved solids (TDS), dyes, chemical oxygen demand (COD), suspended solids (SS), and metals [2]. Dyes are considered the major pollutants in the textile effluent that have had detrimental effects on water resources, the environment, and human health [3]. Hence, nowadays, photocatalytic degradation has been employed to degrade the dyes, whereby aligns with the targets of SDG 6, which contributes to improving water quality and reducing pollution.

Photocatalytic degradation is one of the best ways to get rid of dyes. It is an advanced oxidizing process (AOP) to mineralize the hazardous dye molecules into safer products such as carbon dioxide ($CO_2$), water ($H_2O$), and other organic compounds. Photodegradation can be categorized into homogeneous and heterogeneous photocatalysis. Heterogeneous photocatalysis has been a major area of interest within the AOP due to the ease of separation and recyclability of photocatalysts [4]. Recently, metal oxide semiconductors (MOS) such as oxides of titanium (Ti), zinc (Zn), copper (Cu), vanadium (V), iron (Fe), nickel (Ni), and tin (Sn) have served as photocatalysts in heterogeneous photocatalysis due to their unique properties, including excellent redox potential. Semiconductor metal oxides have a high surface area and abundant active sites that enable the adsorption of reactant molecules. Furthermore, their photosensitive properties with a large band gap enable them to absorb light energy, which excites the valence band to the conduction band, thereby generating electron-hole pairs.

Despite being a stand-alone metal oxide semiconductor, agglomeration occurs during the particle-growth stage due to the absence of physical barriers [5]. Moreover, MOS's limitation as a photocatalyst is its partial recovery from the reactant media [6]. Previous research has established metal oxide nanoparticles on substrates such as silica, glass, cellulose, activated carbon, and chitosan. As a photocatalyst, the metal oxide semiconductor immobilized on the substrate possesses a high surface area along with outstanding stability [7].

Biopolymer-based adsorbents have been endeavoured by numerous researchers for the adsorption of dyes. For example, cellulose/sodium alginate, chitosan/biochar, and alginate/hydrogel have been employed for the adsorption study of different dyes [8-10]. Previous studies reported that these biopolymers were synthesized by bacterial cellulose grafting acrylic acid [11] and the ionic gelation method [12]. In particular, cellulose and chitosan are biopolymers containing hydroxyl and amino functional groups that can form electrostatic forces with dyes [10]. These functional groups allow interaction with dyes via electrostatic interaction and hydrogen bonding. Moreover, they are low-cost and environmentally friendly. However, cellulose has limited adsorption capacity for particular substances and weak mechanical strength, whereas chitosan has limited stability under acidic conditions. Hence, the composition of chitosan-cellulose exhibits superior adsorption capabilities and mechanical properties.

This article explored a novel perspective on understanding the different supporting materials for the functionalization of NiNPs for the photodegradation of dye. It discussed the

potential use of pristine filter paper (FP) and chitosan-filter paper (CS-FP) to enhance the immobilization of NiNPs, thereby improving the removal efficacy of dye. Therefore, this study aims to synthesize NiNPs on FP and CS-FP by the dip-coating method. These substrates were selected for this project due to their abundance, biodegradability, and higher absorption potential. The adsorption ability of the substrates to the NiNPs was investigated by comparing their surface morphology, chemical composition, and functional groups. The photocatalytic performances of NiNPs/FP and NiNPs/CS-FP on methylene blue (MB) were investigated under UV radiation with various parameters. This finding highlights the importance of studying the photodegradation process of NiNPs immobilized on different substrates for the removal of dyes, which may make a meaningful contribution to the achievement of SDG 6.

## 2. MATERIALS AND METHODS

### *2.1 Reagents*

Nickel sulphate hexahydrate ($NiSO_4•H_2O$, 90-100 %) from the supplier Bendoson, sodium pyrophosphate decahydrate ($Na_4P_2O_7•10H_2O$, 97 %) from Acros Organics, silver nitrate ($AgNO_3$, 99 %) from ChemAR®, borane dimethylamine ($(CH_3)_2NH•BH_3$, 98 %) from Thermo Scientific™, methylene blue ($C_{16}H_{18}ClN_3S$, 97 %) from Merck, sodium borohydride ($NaBH_4$, 98 %), and ammonia solutions ($NH_4OH$, 30 %) were sourced from R&M Chemicals. The material used in this study was grade 3 filter paper.

### *2.2 Preparation of NiNPs/FP and NiNPs/CS-FP*

NiNPs/FP and NiNPs/CS-FP were synthesized using the Zeng et al. [13] method with a minor modification. Filter paper was cut into small pieces and rinsed with deionized water prior to use. Pristine filter paper was then immersed in 0.009 M of $AgNO_3$ solution for 30 minutes at room temperature. The NiNPs solution was prepared by dissolving $NiSO_4•H_2O$, $Na_4P_2O_7•10H_2O$, $(CH_3)_2NH•BH_3$, and $NH_4OH$ in 100 mL of deionized water. Afterwards, the FP spent 4 hours submerged in the NiNPs solution. The fabricated NiNPs/FP were rinsed with copious amounts of deionized water and dried for further use.

The chitosan-filter paper (CS-FP) was prepared by immersing the washed filter paper in 2 % (W/V) of chitosan solution for 3 hours. The CS-FP was dried and used as the substrate for the synthesis of NiNPs/CS-FP, as in the previous procedure.

### *2.3 Characterization of Photocatalysts*

Using scanning electron microscopy with energy dispersive X-ray spectroscopy (JEOL JSM IT-200), the particle size and surface morphology of NiNPs/FP and NiNPs/CS-FP were studied. Functional groups in pristine FP, CS-FP, NiNPs/FP, and NiNPs/CS-FP were compared by using Fourier transform infrared spectroscopy (Spectrum 100) equipped with attenuated total reflectance in transmittance mode within the wavelength range of 700-4000 $cm^{-1}$.

### *2.4 Photodegradation Experiment*

The photodegradation of methylene blue (MB) using NiNPs/FP and NiNPs/CS-FP as photocatalysts were conducted under 13 watts of UV light at the desired concentration of sodium borohydride. In this study, sodium borohydride ($NaBH_4$) acts as the reducing agent to enhance the performance of photocatalysts. To attain an adsorption-desorption equilibrium, 0.4 g of photocatalyst was added to 100 mL of MB in a dark condition with ventilation for 1 hour. After adsorption-desorption equilibrium was achieved, 10 mL of $NaBH_4$ at the desired concentration was added to the MB solution, and UV light was switched on to excite the NiNPs photocatalyst. 10 mL of aliquot was drawn after 3 hours of photodegradation. On account of the NiNPs/FP deteriorating during the photodegradation process, sedimentation was necessary to settle the NiNPs/FP debris. The collected aliquot was then examined by a UV-Vis spectrophotometer. In UV-Vis analysis, peaks were observed in the wavelength range between 550 and 750 nm and were assigned to the absorption of the π-system. Then, the decolorization values of the dye solution were calculated using the following Equation (1).

$$D = \frac{C_0 - C_1}{C_0} \times 100\% = \frac{A_0 - A_1}{A_0} \times 100\% \quad (1)$$

where D is the percentage of decolorization and $C_0$, $A_0$ and $C_1$, $A_1$ are the concentration and absorbance of dye solution at maximum wavelength before and after irradiation, respectively.

Photodegradation parameters such as initial concentration of MB, photocatalyst dosage, and concentration of reducing agent were studied to investigate the photocatalytic performances of NiNPs/FP and NiNPs/CS-FP.

## 3. RESULTS AND DISCUSSION

### *3.1 Synthesis of NiNPs/FP and NiNPs/CS-FP*

Figure 1 illustrates the physical appearance of NiNPs/FP and NiNPs/CS-FP. In the fabrication of NiNPs/FP, the pristine FP was immersed in $AgNO_3$ solution, followed by a NiNPs solution. An observation of the transition in colour from white to brown, then black. In this case, the silver ions act as the precursor for the reduction of nickel ions. Conversely, in the fabrication of NiNPs/CS-FP, $AgNO_3$ solution was first applied to the CS-FP and subsequently NiNPs solution. A colour transition that goes from white to brown black to silver black. The hue change can prove that oxidation-reduction reactions occur.


**Figure 1:** Physical appearance of (a) NiNPs/FP and (b) NiNPs/CS-FP

### *3.2 Characterization of Photocatalysts*

SEM analysis was performed to observe the morphological differences of NiNPs on different substrates. The SEM micrographs of NiNPs on pristine FP and CS-FP with different magnifications are revealed in Figure 2. The NiNPs immobilized on FP and CS-FP show an irregular, spherical-like shape with particle sizes in the range of 50–250 nm. It is obviously observed in Figure 2(c) that the surface of the fibre is smoother compared to Figure 2(a) due to the covering of CS film. The NiNPs/CS-FP in comparison to NiNPs/FP indicated less porosity and the small particle size evidently proves that the CS covered the microfibers of FP. There are some aggregates of NiNPs observed on both FP and CS-FP. Even though the vast majority of NiNPs are uniformly dispersed on the substrate surface.

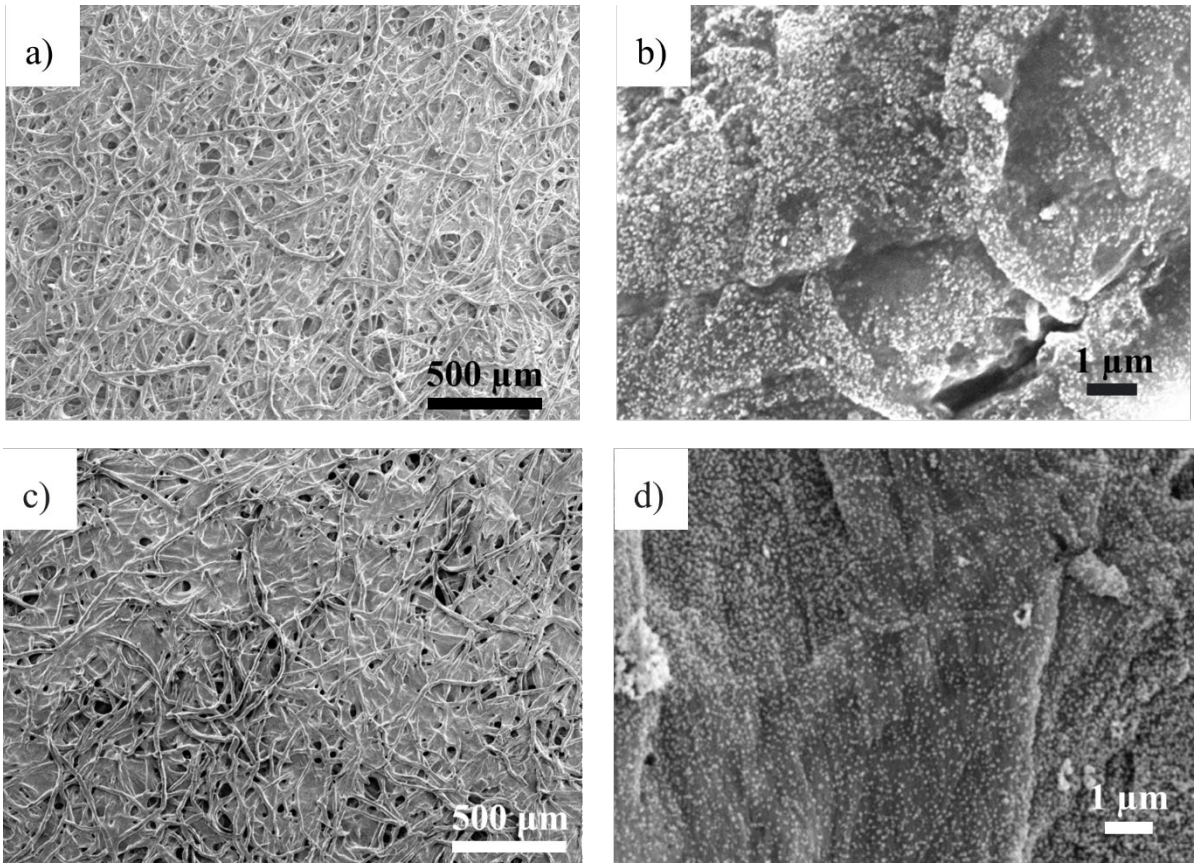


**Figure 2:** SEM micrograph of NiNPs/FP with magnification (a) 50x, (b) 10,000x, and NiNPs/CS-FP with magnification (c) 50x and (d) 10,000x

EDX was implied to verify the successfulness of NiNPs immobilized on both substrates by dipping methods. In Figure 3, elemental analysis shows the atomic percentages of carbon, oxygen, and nickel on FP and CS-FP. The presence of carbon and oxygen elements was revealed due to the organic nature of CS and FP [14]. According to elemental analysis, the Ni element signals were specifically identified, demonstrating the existence of the Ni component in the synthesized NiNPs/CS-FP and NiNPs/FP. NiNPs/CS-FP indicates a higher atomic percentage compared to NiNPs/FP, which are 13.93 % and 2.80 %, respectively. This difference is attributed to the excellent adsorption capacity of metal ions in CS [15].

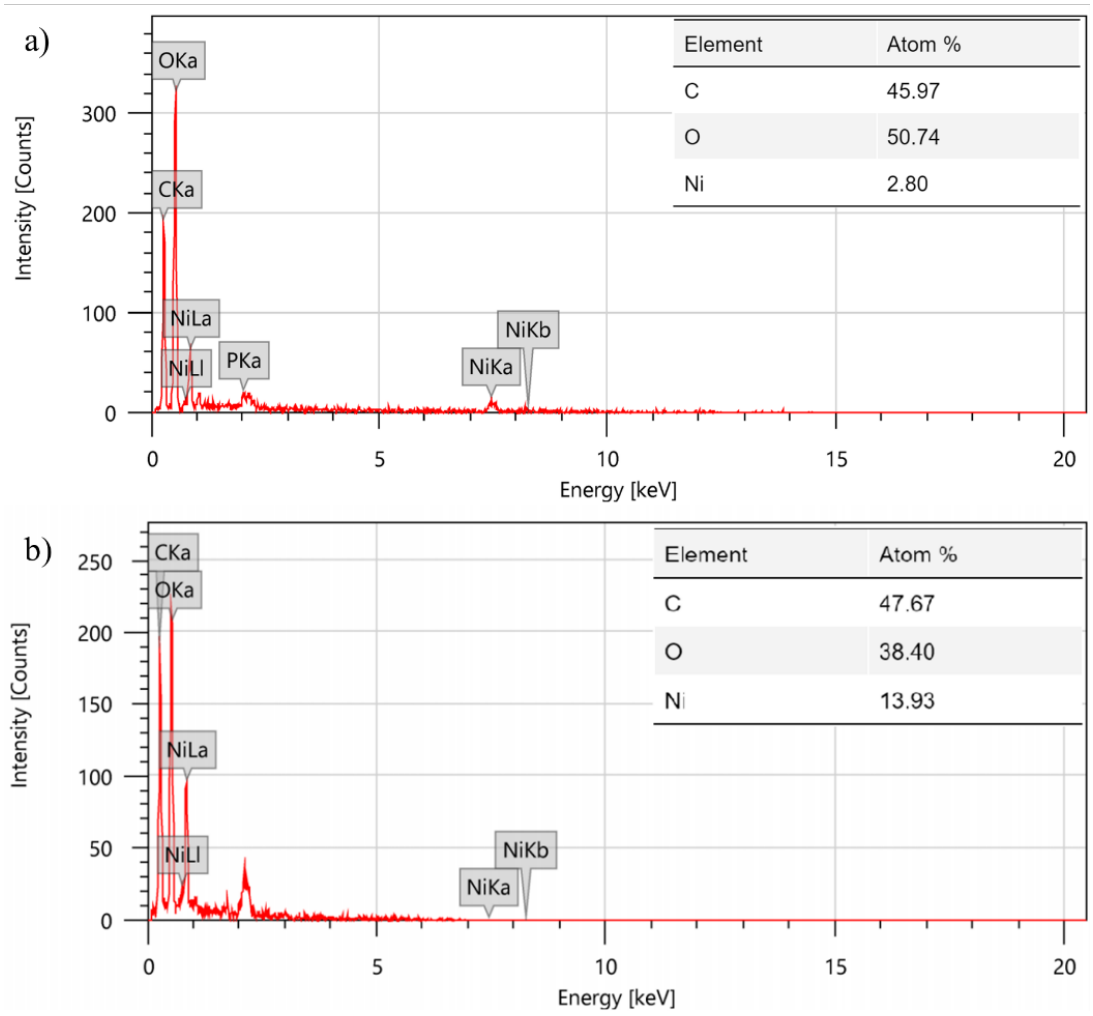


**Figure 3:** The EDX spectra of (a) NiNPs/FP and (b) NiNPs/CS-FP

Figure 4 indicates the FTIR spectra of FP, CS-FP, NiNPs/FP, and NiNPs/CS-FP were characterized over the range of 700–4000 $cm^{-1}$. FTIR confirmed the deposition of CS and NiNPs on the FP. It is evident that the FTIR spectra of FP showed peaks at 3337 $cm^{-1}$ (O-H stretching), 2901 $cm^{-1}$ (C-H stretching), 1639 $cm^{-1}$ (C=C stretching), 1315 $cm^{-1}$ (O-H bending), 1190 $cm^{-1}$ (C-O-C stretching), 1053 and 1029 $cm^{-1}$ (C-N stretching), which are the characteristics of cellulose.

The FTIR spectra of CS-FP, in comparison to FP, have almost similar functional groups. However, the presence of chitosan has led to a decrease in the IR band intensity of CS-FP near 3500-3200 $cm^{-1}$, 1650-1350 $cm^{-1}$, and 1200-1000 $cm^{-1}$. These characteristics provide interactions such as electrostatic attraction and hydrogen bonding between the oxygen-containing functional groups of the substrate and the amino and sulfhydryl groups of MB [16]. In the FTIR spectra for NiNPs/FP and NiNPs/CS-FP, there is a diminishing peak between 3700 and 3500 $cm^{-1}$ due to the immobilization of NiNPs on the substrates. Nevertheless, Feiz et al. [14] reported that there are no huge changes in FTIR spectra compared with pristine FP, CS-FP, and Cu/CS-FP. This is due to the significant influence of the concentration of chitosan coated on the filter paper in the study.

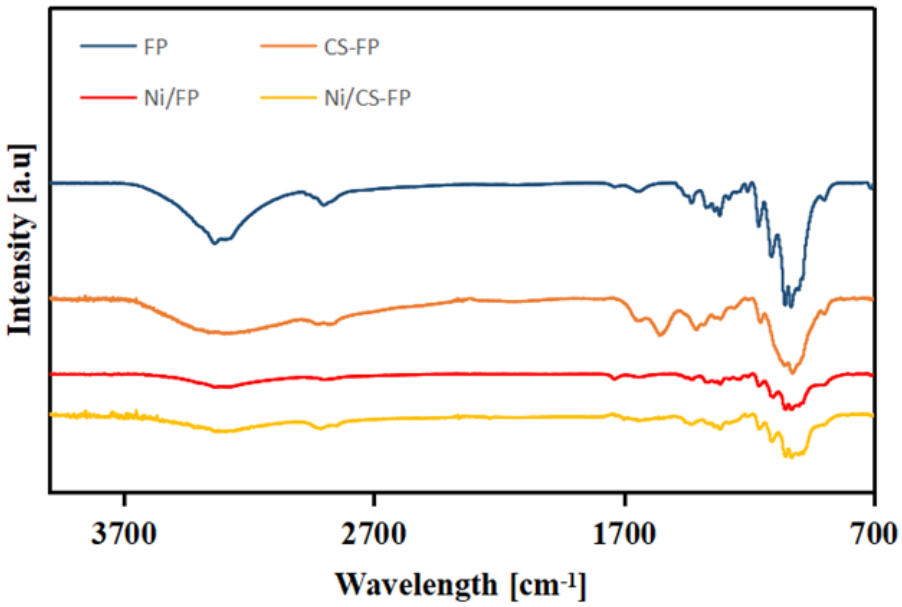


**Figure 4:** The FTIR spectra of FP, CS-FP, NiNPs/FP, and NiNPs/CS-FP

### *3.3 Photodegradation Experiment*

Photodegradation of methylene blue (MB) was carried out to evaluate the photocatalytic performance of NiNPs/FP and NiNPs/CS-FP. MB was used as the model of contamination in the project. Figure 5 compares the effect of photocatalyst (NiNPs/FP and NiNPs/CS-FP) dosage on the photocatalytic degradation of MB. It is apparent from this figure that the photodegradation performance of MB has increased with the increase in photocatalyst dosage. According to the findings, the MB photodegradation efficiency of NiNPs/FP went from 42.8 % to 68.7 %, whereas NiNPs/CS-FP exhibited a rise from 22.4 % to 47.6 %. Theoretically, the photocatalytic degradation performance has a relationship with the photocatalyst concentration. As the photocatalyst loading increases, the photodegradation efficiency increases. This is due to the abundance of available photon absorption centres and activity centres on the active sites [17].

A further increase in the amount of photocatalyst had less impact on the photocatalytic degradation effect of MB. It can be considered that at the photocatalyst dose of 0.6 g, the photodegradation efficiency of MB attained its ideal state. In comparison to NiNPs/CS-FP, a noticeable photodegradation efficiency of MB by NiNPs/FP can be well ascribed to the superior adsorption ability due to high porosity. Moreover, there are free amino and hydroxyl groups in the substrate of NiNPs/FP, which allows electrostatic interaction with MB. On the other hand, NiNPs/CS-FP has less satisfactory free amino and hydroxyl groups for the adsorption of MB.

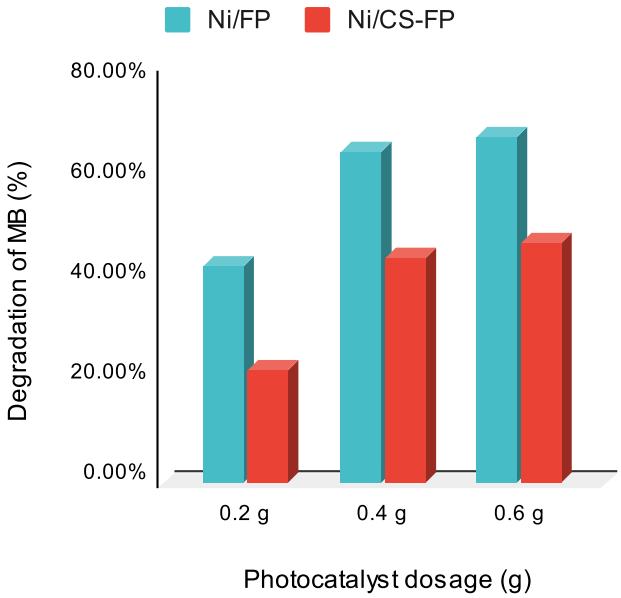


**Figure 5:** Effect of NiNPs/FP and NiNPs/CS-FP dosages on photodegradation of MB

The initial concentration of MB affects the photodegradation performance of NiNPs/FP and NiNPs/CS-FP, as shown in Figure 6. The results elucidated that the photodegradation performance of NiNPs/FP gradually decreased from 67.4 % to 62.8 % with the increment of the initial concentration of MB from 10 ppm to 50 ppm. Conversely, there is an obvious decline in the photodegradation efficiency of MB from 61.4 % (10 ppm) to 44.5 % (20 ppm) and then a gradual decrease to 38.7 % (50 ppm). This may be due to the fact that the adsorption of MB on the active sites of the photocatalysts inhibits the generation of hydroxyl radicals [18]. Another possible cause for the decrease in photodegradation efficiency of MB is the screening of UV light by the high concentration of dyes. The decreasing photocatalytic efficiency of NiNPs/FP in comparison to NiNPs/CS-FP is lower as there are more sites available on NiNPs/FP accessible for dye adsorption.

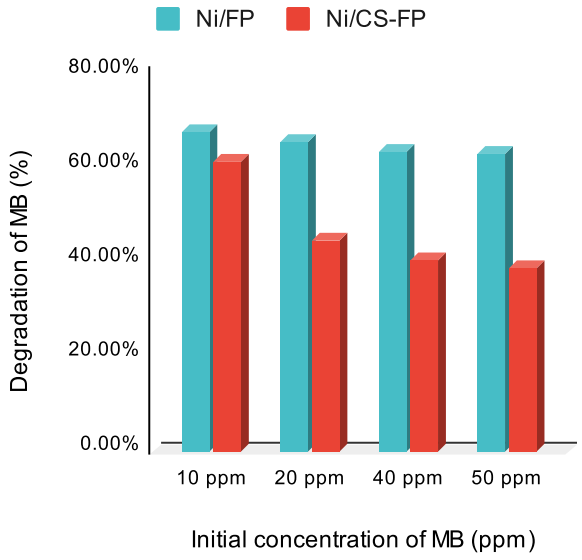


**Figure 6:** Photocatalytic performance of NiNPs/FP and NiNPs/CS-FP with different initial concentrations of MB

The photocatalytic activity of NiNPs/FP and NiNPs/CS-FP were explored in the presence of a series of concentrations of $NaBH_4$ (0, 0.1, 0.3, and 0.5 M). In this project, $NaBH_4$ plays a vital role as a reducing agent. The results show a positive correlation between the photodegradation efficiency of MB and the concentration of $NaBH_4$. What stands out in this chart is that there is a significant difference in photodegradation efficiency of MB between NiNPs/FP and NiNPs/CS-FP at 0 M of $NaBH_4$. Because of their high porosity and the availability of free functional groups for adsorption, NiNPs/FP has a higher removal rate on MB, as previously discussed. With the presence of 0.5 M $NaBH_4$, the optimal photodegradation rate of MB for NiNPs/FP reached 98.2 %, nevertheless, NiNPs/CS-FP achieved only a moderate photodegradation rate of 64.4 %.

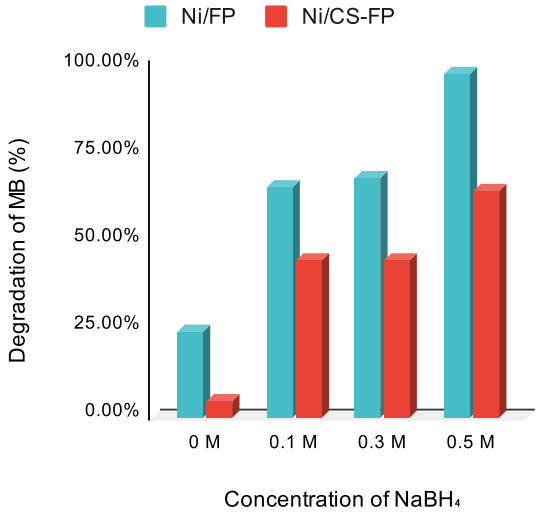


**Figure 7:** Photodegradation performance of NiNPs/FP and NiNPs/CS-FP with different concentrations of $NaBH_4$

## 4. CONCLUSIONS

In this study, NiNPs were immobilized on substrates, which are FP and CS-FP, by the dip-coating method. Instruments such as SEM, EDX, and FTIR have been employed in ascertaining the success of NiNPs immobilized uniformly on substrates as well as comparing the amount of element coated on substrates. A significant proportion of NiNPs have been able to adsorb on CS-FP, attributed to its excellent adsorption capabilities. This study provides a comparison of the photodegradation performance of NiNPs/FP and NiNPs/CS-FP on MB with various parameters such as the photocatalyst dosage, initial concentrations of dye, and concentrations of reducing agent. The study has found that generally, the photocatalytic activity of NiNPs/FP is better than that of NiNPs/CS-FP due to its available site for adsorption of MB. In short, both substrates showed their respective advantages in terms of removing MB and adsorbing nickel.

## Acknowledgements

This work was financially supported by Universiti Malaysia Pahang Al-Sultan Abdullah, Pahang, Malaysia under Post Graduate Research Grant Scheme (PGRS230373).

## Author Contributions

All authors contributed toward data analysis, drafting and critically revising the paper and agree to be accountable for all aspects of the work.

## Disclosure of Conflict of Interest

The authors have no disclosures to declare.

## Compliance with Ethical Standards

The work is compliant with ethical standards.

## References

[1] Zahuri, A. A., Abdul Patah, M. F., Kamarulzaman, Y., Hashim, N. H., Thirumoorthi, T., Wan Mohtar, W. H. M., Mohd Hanafiah, Z., Amir, Z., & Wan-Mohtar, W. A. A. Q. I. (2023). Decolourisation of Real Industrial and Synthetic Textile Dye Wastewater Using Activated Dolomite. *Water (Switzerland),* 15(6).

[2] Wang, X., Jiang, J., & Gao, W. (2022). Reviewing textile wastewater produced by industries: characteristics, environmental impacts, and treatment strategies. *Water Science and Technology* 85(7), 2076–2096.

[3] Lellis, B., Fávaro-Polonio, C. Z., Pamphile, J. A., & Polonio, J. C. (2019). Effects of textile dyes on health and the environment and bioremediation potential of living organisms. *Biotechnology Research and Innovation*, 3(2), 275–290.

[4] Tahir, M. B., Iqbal, T., Rafique, M., Rafique, M. S., Nawaz, T., & Sagir, M. (2020). Nanomaterials for photocatalysis. *Nanotechnology and Photocatalysis for Environmental Applications*, pp. 65–76.

[5] Tsuzuki, T. (2021). Mechanochemical synthesis of metal oxide nanoparticles. *Communications Chemistry,* 4(1).

[6] Bokov, D. O., Mahmoud, M. Z., Widjaja, G., Suksatan, W., Chupradit, S., Altimari, U. S., Hussein, H. A., Mustafa, Y. F., & kazemnejadi, M. (2022). Transfer hydrogenation of nitroarenes using cellulose filter paper-supported Pd/C by filtration as well as sealed methods. *RSC Advances,* 12(18), 10933–10949.

[7] Joseph, A., & Vijayanandan, A. (2023). Review on support materials used for immobilization of nano-photocatalysts for water treatment applications. *Inorganica Chimica Acta,* 545, 121284.

[8] Kausar, A., Rehman, S. U., Khalid, F., Bonilla-Petriciolet, A., Mendoza-Castillo, D. I., Bhatti, H. N., Ibrahim, S. M., & Iqbal, M. (2022). Cellulose, clay and sodium alginate

composites for the removal of methylene blue dye: Experimental and DFT studies. *International Journal of Biological Macromolecules,* 209, 576–585.

[9] Doondani, P., Gomase, V., Saravanan, D., & Jugade, R. M. (2022). Chitosan coated cotton-straw-biochar as an admirable adsorbent for reactive red dye. *Results in Engineering,* 15, 100515.

[10] Asadi, S., Eris, S., & Azizian, S. (2018). Alginate-based hydrogel beads as a biocompatible and efficient adsorbent for dye removal from aqueous solutions. *ACS Omega,* 3(11), 15140–15148.

[11] Luo, M. T., Li, H. L., Huang, C., Zhang, H. R., Xiong, L., Chen, X. F., & Chen, X. de. (2018). Cellulose-based absorbent production from bacterial cellulose and acrylic acid: Synthesis and performance. *Polymers*, 10(7), 702.

[12] Van Bavel, N., Lewrenz, A. M., Issler, T., Pang, L., Anikovskiy, M., & Prenner, E. J. (2023). Synthesis of alginate nanoparticles using hydrolyzed and enzyme-digested alginate using the ionic gelation and water-in-oil emulsion method. *Polymers,* 15(5), 1319.

[13] Zeng, Q., Liu, Y., Shen, L., Lin, H., Yu, W., Xu, Y., Li, R., & Huang, L. (2021). Facile preparation of recyclable magnetic Ni@filter paper composite materials for efficient photocatalytic degradation of methyl orange. *Journal of Colloid and Interface Science*, 582, 291–300.

[14] Feiz, E., Mahyari, M., Ghaieni, H. R., & Tavangar, S. (2021). Copper on chitosan-modified cellulose filter paper as an efficient dip catalyst for ATRP of MMA. *Scientific Reports,* 11(1).

[15] Gamage, A., Jayasinghe, N., Thiviya, P., Wasana, M. L. D., Merah, O., Madhujith, T., & Koduru, J. R. (2023). Recent application prospects of Chitosan based composites for the metal contaminated wastewater treatment. *Polymers*, 15(6), 1453.

[16] Athari, M., Fattahi, M., Khosravi-Nikou, M., & Hajhariri, A. (2022). Adsorption of different anionic and cationic dyes by hybrid nanocomposites of carbon nanotube and graphene materials over UiO-66. *Scientific Reports,* 12(1).

[17] Zhang, D., Lv, S., & Luo, Z. (2020). A study on the photocatalytic degradation performance of a $[KNbO_3]_{0.9}$-$[BaNi_{0.5}Nb_{0.5}O_{3-\delta}]_{0.1}$ perovskite. *RSC Advances,* 10(3), 1275–1280.

[18] Badvi, K., & Javanbakht, V. (2021). Enhanced photocatalytic degradation of dye contaminants with $TiO_2$ immobilized on ZSM-5 zeolite modified with nickel nanoparticles. *Journal of Cleaner Production,* 280, 124518.